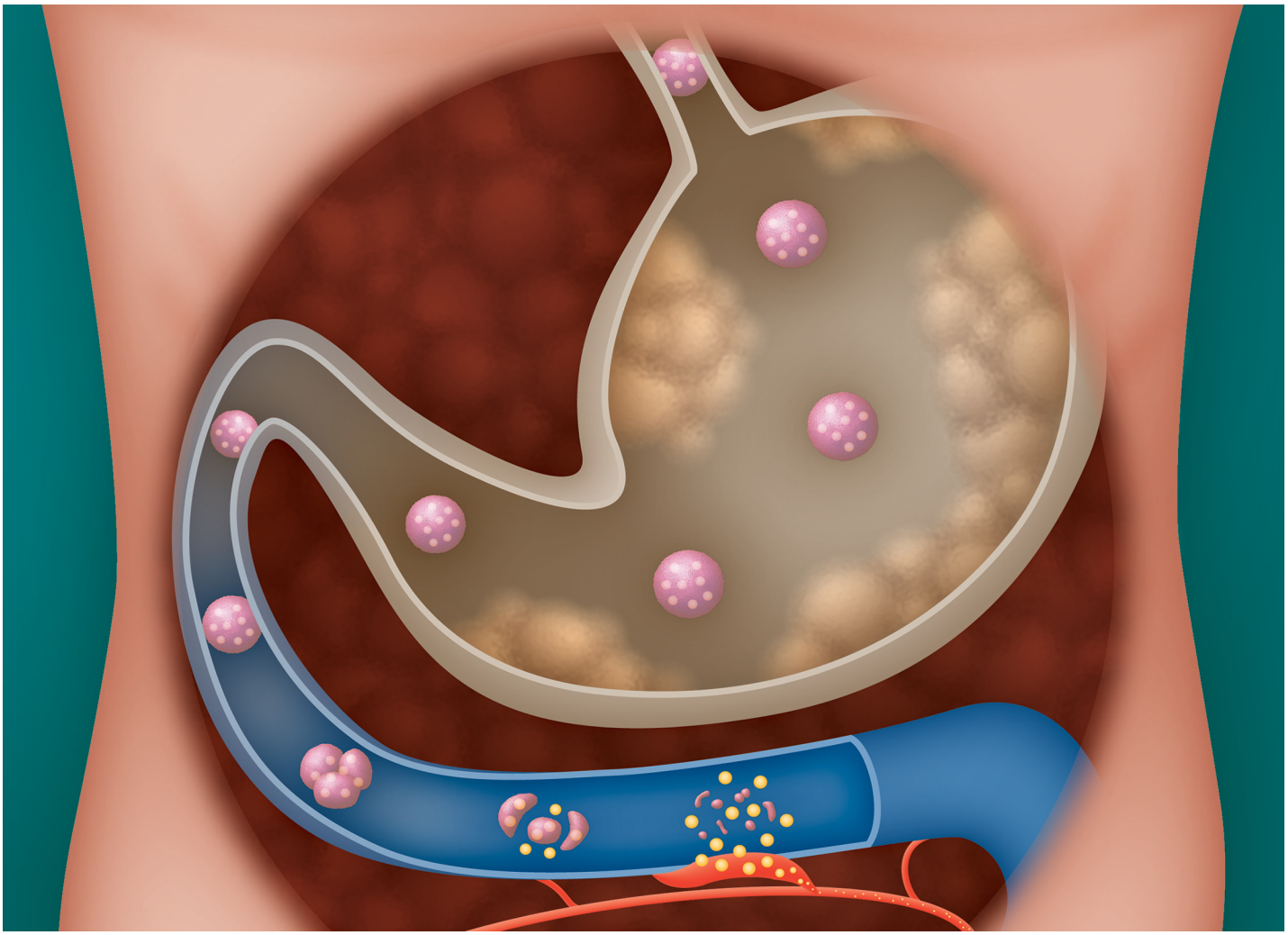

Showcasing research from Professor Hang T. Ta's laboratory, Queensland Micro and Nanotechnology Centre, School of Environment and Science, Griffith University, Brisbane, Australia.

Poly(succinimide) nanoparticles as reservoirs for spontaneous and sustained synthesis of poly(aspartic acid) under physiological conditions: potential for vascular calcification therapy and oral drug delivery

We have developed biocompatible nanoparticles based on poly(succinimide) that are stable at low pH and gradually dissolve at physiological pH, which is a highly desirable feature for oral drug delivery. During dissolution, polysuccinimide converts to poly(aspartic acid) that can effectively prevent calcification of smooth muscle cells. Overall, the developed nanomaterials have great potential for drug delivery and vascular calcification treatment.

As featured in:

See Hang Thu Ta *et al.*, *J. Mater. Chem. B*, 2023, **11**, 2650.

ROYAL SOCIETY OF CHEMISTRY

rsc.li/materials-b

Registered charity number: 207890

Journal of Materials Chemistry B

ROYAL SOCIETY OF CHEMISTRY

PAPER

Cite this: *J. Mater. Chem. B*, 2023, **11**, 2650

Poly(succinimide) nanoparticles as reservoirs for spontaneous and sustained synthesis of poly(aspartic acid) under physiological conditions: potential for vascular calcification therapy and oral drug delivery†

Hossein Adelnia,[ab] Idriss Blakey,[be] Peter J. Little[d] and Hang Thu Ta *[abc]

Received 1st September 2022,
Accepted 13th January 2023

DOI: 10.1039/d2tb01867e

rsc.li/materials-b

This paper describes the preparation of poly(succinimide) nanoparticles (PSI NPs) and investigates their properties and characteristics. Employing direct and inverse precipitation methods, stable PSI NPs with tunable size and narrow dispersity were prepared without the use of any stabilizer or emulsifier. It was demonstrated that PSI NPs convert to poly(aspartic acid) (PASP) gradually under physiological conditions (37 °C, pH 7.4), while remaining stable under mildly acidic conditions. The dissolution profile was tuned and delayed by chemical modification of PSI. Through grafting a fluorophore to the PSI backbone, it was also demonstrated that such a spontaneous conversion could offer great potential for oral delivery of therapeutic agents to the colon. Sustained PASP synthesis also contributed to a sustained reduction of reactive oxygen species induced by iron. Furthermore, PSI NPs effectively prevented *in vitro* calcification of smooth muscle cells. This was attributed to the chelation of calcium ions to PASP, thereby inhibiting calcium deposition, because under cell culture conditions PSI NPs serve as reservoirs for the sustained synthesis of PASP. Overall, this study sheds light on the preparation and features of biocompatible and biodegradable PSI-based NPs and paves the way for further research to discover as-yet unfulfilled potential of this polymer in the form of nanoparticles.

Introduction

In recent years, PASP has found a wide variety of applications in different fields due to its attractive characteristics. As an anionic polypeptide with protein-like bonds in each polymer repeat unit, PASP is highly biocompatible and biodegradable.[1] It also has a strong affinity to metal ions such as calcium, iron and copper.[2] Strong metal complexation of PASP could potentially be used in chelation therapy, reduction of heavy metal toxicity and other areas as recently reviewed by us.[2] Lightly crosslinked PASP hydrogels can uptake large amounts of water. Due to its anionic nature, PASP and its corresponding gels respond to pH changes and thus can be utilized as smart stimuli-responsive hydrogels.[3,4]

Both in small and large scales, PASP is typically obtained by alkali hydrolysis of its precursors, that is poly(succinimide) (PSI).[5] In addition to alkali hydrolysis, the succinimide rings of PSI can be opened by primary amines, yielding polyaspartamides, allowing one to modify PSI/PASP with a wide variety of species ranging from polymers to drugs.[6] Jalalvandi *et al.*[5] reviewed chemical modification of PSI and reported that the resulting compounds can be degraded into short chain peptides or amino acids in the body. On the basis of such chemical modification, PSI has so far been employed to prepare PASP or polyaspartamides for the preparation of drug delivery systems,[7] magnetic resonance imaging (MRI) contrast agents,[8] dispersants,[9] and beyond.[1–3,5,6]

PSI could also be hydrolyzed to PASP under milder condition (*e.g.*, neutral pH) but at a much slower rate.[10] While PASP generally dissolves well in water, PSI is highly water insoluble, enabling one to prepare its solid (nano)particles dispersible in physiological media. In light of this and considering its tendency to hydrolysis, we were motivated to synthesize PSI nanoparticles

[a] *Queensland Micro- and Nanotechnology Centre, Griffith University, Brisbane, 4111, Queensland, Australia. E-mail: h.ta@griffith.edu.au; Tel: +61 (7) 3735 5384; Web: https://hangta.group/, https://experts.griffith.edu.au/27034-hang-ta*
[b] *Australian Institute for Bioengineering and Nanotechnology, University of Queensland, St Lucia, Brisbane, 4067, Queensland, Australia*
[c] *School of Environment and Science and Queensland Micro- and Nanotechnology, Griffith University, Nathan Campus, Brisbane, 4111, Queensland, Australia*
[d] *School of Pharmacy, the University of Queensland, Brisbane, 4102, Queensland, Australia*
[e] *Centre for Advanced Imaging, University of Queensland, Brisbane, 4067, Queensland, Australia*

† Electronic supplementary information (ESI) available. See DOI: **https://doi.org/10.1039/d2tb01867e**

(PSI NPs) to evaluate their dissolution/degradation, and conversion to PASP, especially under physiological conditions. As such, first, the preparation of PSI NPs was conducted by a nanoprecipitation method, in either a direct or inverse manner. To achieve well-defined PSI NPs, the effects of different parameters on the size, dispersity, and colloidal stability were investigated.

The PSI-to-PASP conversion opens up a wide window for PSI NPs to be exploited for treatment of different diseases, not only *via* its application as a carrier of therapeutic agents, but also *via* the bioactivity of PASP as a biocompatible, biodegradable anionic homo-polypeptide, which has exhibited great promise as a chelating agent of different metal ions (*e.g.*, Ca, Pb, and Cu).[2] Regarding the former, this study investigates the release of a fluorophore grafted on the backbone of PSI under different pH conditions to evaluate its response in the gastrointestinal tract. Regarding the latter, this study also assesses the effect of PSI NPs on *in vitro* calcification of vascular smooth muscle cells induced by β-glycerophosphate. Furthermore, it is suggested that sustained synthesis of PASP under physiological conditions could be used for lowering ROS levels induced by iron overload.

Experimental section

Materials

L-Aspartic acid (ASP), sulfolane, phosphoric acid, methanol, sodium hydroxide, dimethyl sulfoxide, *N*,*N*-dimethylformamide (DMF), oleylamine (OA), ethylenediamine (EDA), DMF were all purchased from Sigma Aldrich and used without further purification.

Synthesis of PSI

PSI was synthesized through a poly-condensation reaction of ASP monomer at 180 °C under nitrogen atmosphere for 5 hours in the presence of phosphoric acid as a catalyst as shown in Scheme 1. Sulfolane was used as the polymerization solvent. In a typical reaction, ASP (14 g), H_3PO_4 (0.98 g), and sulfolane (56 g) were poured into a flask placed in an oil bath at 180 °C under gentle stirring (250 rpm, overhead mechanical stirrer, IKA RW 20 Digital) and gentle flow of nitrogen. After the reaction (5 hours), the product was precipitated into deionized (DI) water. The polymer powder was washed several times with DI water to remove excess catalyst, and solvent. The yield was measured by weighting the dry polymer and found to be comparable to that of monomer, confirming complete polymerization of the monomer.

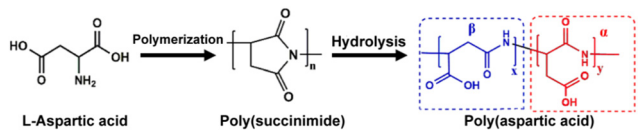

Scheme 1 Poly-condensation reaction of ASP at 180 °C under nitrogen atmosphere for 5 hours, yielding PSI (also known as polyanhydroaspartic acid). The alkali hydrolysis of the resulting polymer yields PASP. The hydrolysis can occur through either of carbonyl groups on the succinimide ring, resulting in a mixture of α and β PASP.

Hydrolysis of PSI to PASP

Alkali hydrolysis of PSI yields PASP as shown in Scheme 1. In a typical reaction, an excess of sodium hydroxide (1.2 times) with respect to moles of succinimide groups was added to PSI powder in water in order to ensure complete hydrolysis. In a typical hydrolysis reaction, PSI powder (100 mg) (M_w of succinimide = 97 g mol^{-1}) was added to 20 mL of water containing NaOH (50 mg) (M_w = 40 g mol^{-1}) and incubated at room temperature for two hours. Then, the product was precipitated in methanol and washed several times to remove excess NaOH. The prepared polymer is sodium salt of PASP (*i.e.*, sodium polyaspartate, Na-PASP).

Chemical structure of the synthesized polymer (*i.e.*, PSI) was evaluated by Fourier-transform infrared spectroscopy (FTIR) (Nicolet 5700 FT-IR) and proton nuclear magnetic resonance (^{1}H-NMR) (Model Bruker Ascend 400 MHz NMR spectrometer), operating at 400.13 MHz. The molecular weight of the prepared PASP was determined using an aqueous gel permeation chromatography (GPC) Agilent GPC/SEC with a dual angle laser light scattering detector, viscometer, and differential refractive index detector calibrated using polyethylene oxide standards. FTIR, and ^{1}H-NMR spectra of PSI and PASP are provided in Fig. S1 and S2 (ESI†). Thermal properties are also presented in Fig. S3 (ESI†).

Preparation of PSI NPs by direct precipitation method

In a typical precipitation procedure, 100 mg of PSI was dissolved in 900 μL DMSO (10 wt%). The prepared solution was slowly (200 μL min^{-1}) injected using a micro-syringe pump to 9 mL of DI water (Fig. 1). The mixture was stirred using a high-speed homogenizer (Model Ultra Turrax, T25 IKA-Werke) at rate of 13 500 rpm. After complete injection of the solution, the mixture was further stirred at the same rate for 2 min. The NPs were centrifuged (Model Heraeus Multifuge X1R) at 14 000 × *g* and washed twice with DI water. Dynamic light scattering (DLS) (Zetasizer Nano ZS) was employed to determine the particle size and zeta potential of the particles. Transmission electron microscopy (TEM) images were taken on a JEOL-JEM-1010 TEM, operating at an accelerating voltage of 100 kV.

Preparation of PSI NPs by inverse precipitation method

8 mL of medium was added slowly to 2 mL of PSI solution in DMSO in a 20 mL glass vial. The medium is water unless otherwise specified. The medium was added by a micro-syringe pump at a rate of 600 μL min^{-1} to the polymer solution under stirring with a magnetic stirrer (1500 rpm, size of magnet bar: 3 mm) (Fig. 2). To tune size and stability, PSI with varying concentrations ranging from 0.375 wt% to 10 wt% was used. After 1–2 mL of the medium was injected to the solution, the mixture became bluish in color, indicating the initiation of nucleation or PSI chain through precipitation. After complete precipitation, the samples were washed twice with water to remove DMSO, followed by 30 s of probe sonication at 30% amplitude (Sonics Model VibraCell).

Conjugation of PSI by Cy-5-NH_2 and the release study

Cy5-NH_2 (10 μL, 4 mM in DMSO) was added to PSI solution (500 μL, 50 mg mL^{-1}), and gently stirred overnight at room temperature.

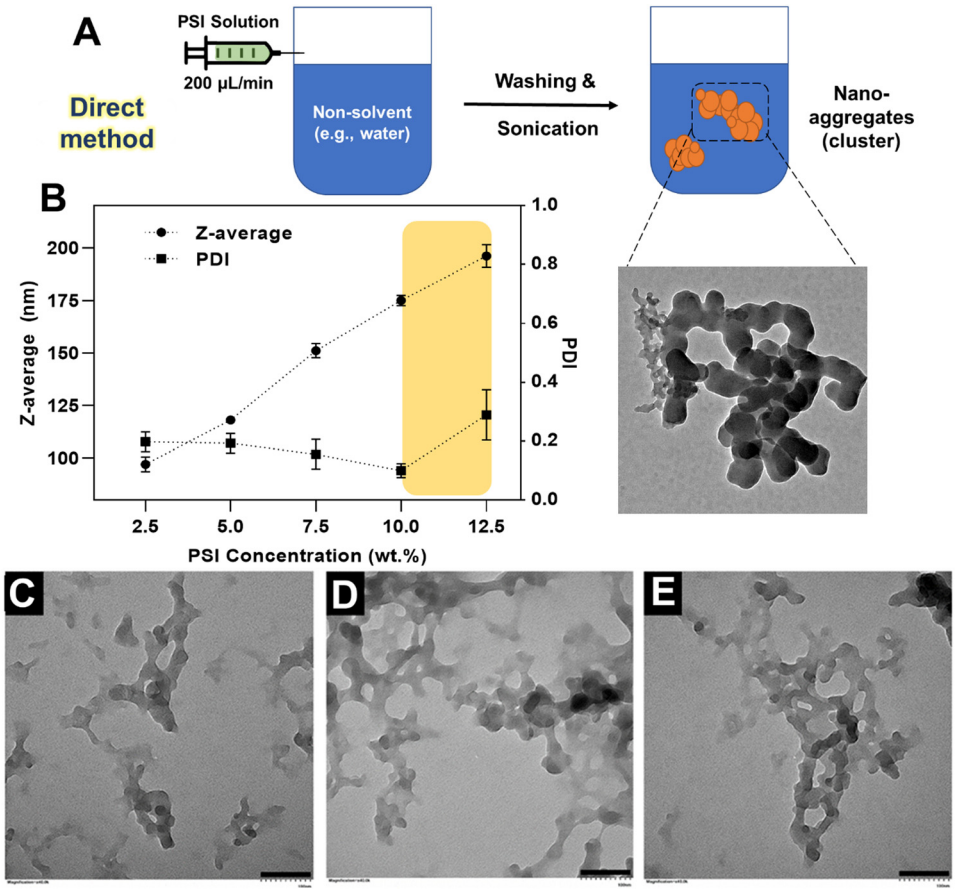

Fig. 1 Preparation of PSI NPs by direct nanoprecipitation. (A) Schematic representation of direct method where polymer solution in DMSO was injected to water as the poor-solvent for PSI. (B) Hydrodynamic diameter (expressed by *z*-average) of the PSI NPs as a function of PSI concentration. The yellow rectangle in the graph shows the concentration range where severe aggregation occurred. For the direct method, the highest tested concentrations where stability was achieved are 10 wt%. The reported values are the mean of 3 dynamic light scattering measurements. (C–E) TEM micrographs of PSI NPs prepared by direct method at PSI concentration (in wt%) of (C) 5, (D) 7.5, (E) 10. Scale bars are 100 nm.

The solution was then precipitated in 10 mL of EtOH and washed twice to remove un-reacted Cy5-NH_2. The polymer was then dried overnight in a vacuum oven at 50 °C. Then, 2 mL of Cy5-conjugated PSI solution at concentration of 6.25 mg mL^{-1} in DMSO was prepared and subjected to the inverse precipitation method described above (precipitation in 8 mL of water at injection rate of 600 μL min^{-1}). The prepared NPs were washed with DI water 2 times. The NPs were then dispersed (final concentration of 500 μg mL^{-1}) in different pH conditions and incubated at 37 °C. Acetate buffer (0.05 M) was used for pH 4.5, whereas phosphate-buffered solution was used for pH 8 and 7.4. At different time intervals, a sample (200 μL) was taken, and centrifuged at 15 000 × *g* for 15 min. The supernatant was gently taken from the pellet and the fluorescent intensity was measured (ex./em. 678/694 nm) by an Omega BMG plate reader.

Preparation of PSI NPs with EDA and OA

Various approaches were adopted to achieve delayed initiation of the dissolution as summarized in Fig. S4 (ESI†). They are generally divided into EDA crosslinking or modification of PSI with OA. The procedure for particle preparation was either direct or inverse precipitation method mentioned above. As seen in Fig. S4 (ESI†), when EDA was added to the preformed PSI NPs, irrespective of used method (direct or inverse) the particles degraded especially at high concentrations (>7.5%) of EDA and thus was not regarded as a suitable approach. It was found that EDA should be added to PSI solution not to PSI NPs. Therefore, in a typical experiment, EDA (1.85 μL) was added to 1 mL of PSI solution (10 wt% in DMSO) followed by conducting the nanoprecipitation quickly. Similar to the above-mentioned, 1 mL of the PSI-EDA solution in DMSO was added to 9 mL of DI water with the injection rate of 200 μL min^{-1} during which the mixture was stirred by a high-speed homogenizer (13 500 rpm), followed by 2 more mins of stirring after completion of the injection. After washing, the PSI NPs (5 mg mL^{-1}) were incubated at 60 °C for 4 h.

Regarding the modification with OA, in a typical reaction, 10 mL of 10 w/v% of PSI in DMF was mixed with 995 μL of OA and incubated under nitrogen atmosphere at 70 °C for 12 hrs. The degree of OA modification was 30% with respect to succinimide units, considering the yield of 100%. After 12 h, the mixture was cooled, the polymer was washed with methanol to remove un-reacted OA as well as excess DMF, and finally the polymer was freeze-dried. Regarding nanoprecipitation

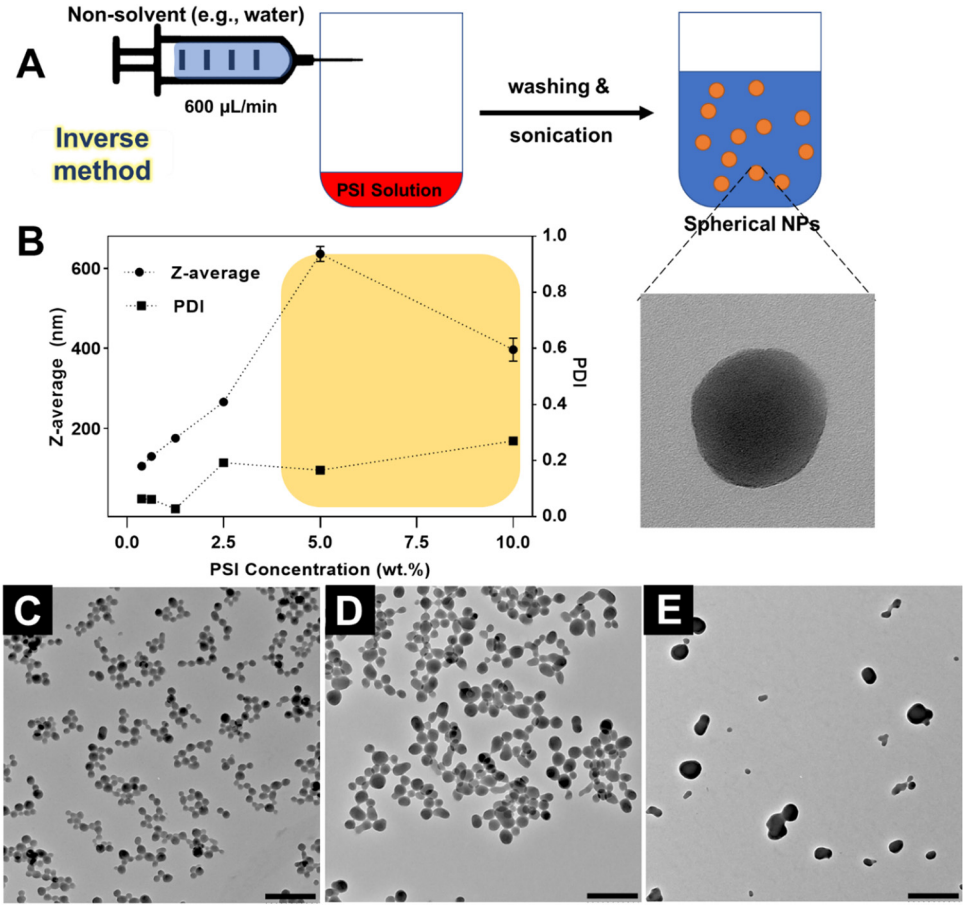

Fig. 2 Preparation of PSI NPs by inverse nanoprecipitation. (A) Schematic representation of inverse method where the poor-solvent (*e.g.*, water) is injected to the polymer solution. (B) Hydrodynamic diameter (expressed by *z*-average) of the PSI NPs as a function of PSI concentration. The yellow rectangle in the graph shows the concentration range where severe coagulation occurs. The reported values are the mean of 3 dynamic light scattering measurements. (C–E) TEM micrographs of PSI NPs prepared by inverse methods. PSI concentration (in wt%) of (C) 0.625, (D) 1.25, and 2.5 (E). Scale bars are 500 nm.

(both direct and inverse), the same procedure was adopted as mentioned above. In a typical direct precipitation, 100 mg of PSI-OA30 was dissolved in 1 mL DMSO and injected at 200 μL min^{-1} while stirring with a homogenizer (rate 8000 rpm). High rate of homogenizer leads to the large foam formation and should be avoided. The particles were washed with DI water several times and used for dissolution study without any further treatment.

For the inverse method, 2 mL of PSI-OA solution (0.625 wt%) in DMF was added to a 20 mL vial. Then DI water with the rate of 600 μL min^{-1} was added to the solution while the solution/mixture was stirring with a magnetic stirrer (1500 rpm). After complete precipitation, the samples were washed 2 times with water to remove DMSO and the particles were used without further treatment for the dissolution studies.

Dissolution study of PSI particles under different conditions

In a typical dissolution experiment, PSI nanoparticle dispersion (2 mg mL^{-1}, 20 μL) were added to phosphate buffer solution (PBS) (180 μL) with different pH values. The mixture was transferred to a 96 well plate. The plate was placed in microplate reader operating at 37 °C (SpectroStar Nano, Model BMG LabTech) and the optical density (OD) spectra was captured in 220–800 nm wavelength range. To evaluate and compare dissolution, OD values at 350 nm as reference were obtained and plotted against time.

Cell viability assay

Cell viability was determined using PrestoBlue cell viability reagent (Invitrogen). Macrophages (J774A.1, ATCC TIB-67) passage of 12, vascular smooth muscle cells (MOVAS, ATCC CRL-2797) passage of 4, as well as endothelial cells (SVEC4-10, ATCC CRL-2181) passage of 5 were seeded in 96-well tissue-treated plates at a density of 5000 cells per well. The media for J774 was RPMI (Sigma 1640) supplemented with fetal bovine serum (FBS) (10%), penicillin–streptomycin (100 U mL^{-1}), and L-glutamine (1%). For MOVAS and SVEC, DMEM (Sigma D6046, 1000 mg per L glucose) supplemented with FBS (10%), and penicillin–streptomycin (100 U each per mL) was used. The cells were cultured and incubated at 37 °C with 5% CO_2. After 24 h incubation in 96 well-plates, the cells were treated with PSI NPs at different concentrations ranging from 10 to 1000 μg mL^{-1}. After 24 h, the medium was aspirated, followed

by adding 100 μL of PrestoBlue solution (diluted 10 times with the PBS). The cells were then incubated at 37 °C for 30 min. Fluorescence intensity was measured at the excitation and emission wavelength of 535 nm (25 nm bandwidth) and 615 nm (10 nm bandwidth), respectively using an Omega BMG plate reader. The background fluorescence value containing no-cell control wells was subtracted from the fluorescence value of each experimental well. Cell viability was calculated by dividing the fluorescence intensity of the sample (The NP-treated) to that of live control (without treatment *i.e.*, standard medium). Dead control is the treated cells with 30% of methanol for 30 min at 37 °C.

Regarding the live/dead cell imaging, calcein AM (5 μL) and ethidium homodimer-1 (EthD-1) (20 μL) were added to 10 mL DPBS and mixed well to create the staining solution. The former and the latter respectively stains the live and dead cells green and red. After removing the cell medium, the staining solution (100 μL) was added to each well and incubate for 30 min at room temperature. The fluorescence images of the cells were taken.

Hemocompatibility assay (RBCs)

Fresh blood was centrifuged at 1000 rpm for 15 min with the lowest acceleration and deceleration rates, to separate plasma with red blood cells (RBCs). After removing the supernatant (*i.e.*, plasma), the obtained RBCs were washed twice with PBS pH 7.4 at 1000 rpm for 15 min (lowest acceleration and deceleration). A stock of RBCs was then prepared by 50 times dilution of 1 mL of washed RBCs with PBS pH 7.4. 100 μL of the PSI NPs at different concentrations and 900 μL of the washed RBCs solution were gently mixed in an Eppendorf tube. Triton-X 100 (1 wt%) and PBS pH 7.4 were used as positive and negative control groups, respectively. The samples were then incubated at 37 °C for 4 h without shaking or stirring. After incubation, the tubes were centrifuged at 14 000 × *g* for 15 min and the supernatant was transferred to a 96-well plate for measuring the absorbance at 545 nm. Hemolysis (%) was calculated according to the equation below:

$$\text{Hemolysis}\,(\%) = \frac{\text{OD sample} - \text{OD negative control}}{\text{OD positive control} - \text{OD negative control}} \times 100$$

Calcification of MOVAS and measurements of calcium, protein and alkaline phosphatase

For *in vitro* calcification, MOVAS cells were seeded into 96-well plates at a density of 5000 cells per well. One day after seeding the cells, treatments of the cells with calcification inducers and polymer were started. The calcification medium was the growth medium stated above supplemented with βGP 10 mM, $CaCl_2$ 1 mM, and ascorbic acid 50 μg mL^{-1} (referred to as βGP control). Calcification medium containing the PSI NPs (up to 100 ppm) was added to and cells and the medium was changed every 3 days. After 12 days of incubation, the medium was aspirated, followed by washing cells with dPBS. After 15 mins of incubation at 37 °C with Tryple Express, the cells were detached, and used for further steps. To measure protein, 50 μL of 2 wt% Triton X-100 (without acid) were added, followed by incubation at 37 °C for 1 h. However, to measure calcium, 50 μL of 2% Triton X-100 in 1.2 M HCl was added to the wells and the mixture was incubated at 37 °C for 1 h. Triton X-100 lyses the cells while HCl dissolves all calcium salts. Calcium concentrations were obtained by a calcium colorimetric assay kit (Sigma, MAK022) by measuring the absorbance at 575 nm.

Alkaline Phosphatase (ALP) Diethanolamine Activity Kit (Sigma AP0100) was used to measure the ALP level in the cell lysate. The assay uses *p*-nitrophenyl phosphate (pNPP) as substrate which is converted to ionic phosphate and *p*-nitrophenol in the presence of ALP. *p*-Nitrophenol has a yellow color and a linear standard curve in the range of 0.0625 to 0.5 unit per mL of ALP was achieved at 405 nm. 20 μL of the sample or standard ALP solutions, 160 μL of the buffer reagent, and 20 μL of freshly prepared *p*-nitrophenyl phosphate (*p*NPP) (67 mM in DI water) were mixed, incubated in dark at room temperature for 30 min, and absorbance was recorded at 405 nm. The ALP level was normalized to the calculated protein level by BCA assay.

Alizarin red staining

After 12 days of incubation, the cells were washed with dPBS and fixed with 4% paraformaldehyde solution in dPBS for 15 min at room temperature. Then, the cells were washed with dPBS twice and a freshly prepared and filtered solution of alizarin red (100 μL, 1 wt% in DI water, pH = 4.1) was added to the wells. The cells were incubated for 10 min at room temperature and the staining solution was aspirated. The cells were washed twice with dPBS and were observed with an inverted optical microscope (CKX53, Olympus). To quantify the calcium deposition through this staining, calcium-alizarin red complex was dissociated with 10 vol% of acetic acid after which a yellowish color was generated. The OD at 422 nm was measured and normalized to the highest value.

Sustained iron chelation of PSI NPs through Fenton reaction

PSI NPs with initial concentration of 200 ppm in PBS pH 7.4 were incubated at 37 °C and a sample was taken at different time intervals. In a 96-well plate, 40 μL of the taken sample was added to 40 μL of iron solution (Fe II or Fe III- 160 μM initial concentration, respectively from $FeCl_2$ $4H_2O$, and $FeCl_3$ $6H_2O$) dissolved in the acetate buffer (sodium acetate/acetic acid, 0.1 M, pH 4.5). This stops the hydrolysis reaction of PSI NPs by lowering the pH. Then, H_2O_2 (40 μL, 1 mM) and finally ABTS solution (40 μL, 1 mM) were added. Both H_2O_2 and ABTS were made in acetate buffer pH 4.5, 0.1 M. The final concentrations of iron, H_2O_2 and ABTS in the well were equal to 40 μM, 250 μM, and 250 μM, respectively while that of PSI/PASP is 50 μg mL^{-1}. The mixture was incubated at 37 °C for 30 min and the absorbance at 414 nm was recorded.

Statistical analyses

Data are presented as the mean ± SD from at least three independent experiments and analyzed with two-way ANOVA. The level of statistical significance was defined as p-value < 0.05.

GraphPad Prism 9 (Graph Pad Prism Inc. CA, USA) was used for plotting the graphs and statistical analysis.

Results and discussion

Preparation of PSI NPs by precipitation method

PSI was synthesized by a poly-condensation method (Scheme 1) and the characterization results are presented in Fig. S1–S3 (ESI†). Preparation of PSI NPs with well-defined size and narrow dispersity is challenging due to the insolubility of PSI in virtually all water-immiscible solvents (*e.g.*, dichloromethane, and ethyl acetate). This makes the implementation of emulsion-based techniques practically impossible unless the polymer is chemically modified, which could be associated with adverse effects on the final properties. To overcome this problem a nanoprecipitation method (also referred to as solvent exchange) was adopted in this study. In a typical procedure, the polymer solution was slowly mixed with a poor solvent for the polymer in the presence of a polymeric stabilizer such as polyvinyl alcohol or polyvinylpyrrolidone.[11] As the polymer solubility was reduced by the added non-solvent, the polymer chains undergo a conformational change from extended to collapsed state, leading to particle formation. The stabilizer typically provides steric hinderance and provides colloidal stability. The good solvent and poor solvent for PSI should be miscible so that no liquid–liquid phase separation or emulsification occurs.[11] Although the addition of polymer solution to the non-solvent (*i.e.*, direct method, shown in Fig. 1) is the most widely adopted and established procedure in nanoprecipitation, we herein investigated the inverse process as well, where the poor solvent is added slowly to the polymer solution (Fig. 2).

In the direct method, the polymer solution in DMSO with varying concentration was added slowly to a large amount of water as the poor solvent (Fig. 1A). This method yielded cluster shape aggregates consisting of several small nanoparticles (Fig. 1A) which could be due to instantaneous collapse of PSI chains upon sudden exposure to water. The results in terms of size, PDI, and zeta potential are presented in Table S1 (ESI†). When the PSI concentration was decreased from 10 to 2.5 wt%, the size decreased from 175 nm to 97 nm (Fig. 1B–E). When the concentration was lower than 2.5 wt%, polymer precipitation and thus particle formation did not occur. On the other hand, highly concentrated solutions deteriorated the colloidal stability to an extent that irreversible and severe aggregation occurred at 15 wt% of PSI.

The inverse method, however, produced spherical particles particularly at a concentration less than 1.25 wt% (Fig. 2). Since the non-solvent was injected slowly in the inverse process, precipitation occurs at a much slower rate, providing the chains with enough time for conformational re-arrangement and particle nucleation which is the reason for spherical shape NPs. Although the shape became more irregular at higher concentrations (>1.25 wt%), no cluster-like aggregates were observed (Fig. 2C–E). Similar concentration dependency in terms of size and stability was also observed using the inverse method, where the size decreased by as much as 160 nm when the concentration decreased from 2.5 wt% to 0.375 wt% (Fig. 2B). Highly stable particles with low dispersity were obtained up to a concentration of 2.5 wt%. However, at 5 wt%, around 20% of the sample aggregated (estimated by filtering). Similar trends have been reported for the concentration-size relationship in the nanoprecipitation of other polymeric systems, such as poly(lactic-*co*-glycolic acid),[12] polycaprolactone,[13] as well as cellulose-based polymers.[14,15]

Overall, the colloidal stability in the absence of stabilizer can be attributed to the functional end groups of PSI which are carboxylic acid (COOH) and amine (NH_2) groups, arising from the ASP monomer. Regardless of the method used, zeta potential values of the NPs at pH values of 3, 5.8, 7.4 and 8.5 were respectively measured to be −15.2, −23.6, −27.2, and −31.8 mV, characterizing the particles as anionic type with negative charges on the surface which are responsible for electrostatic repulsion and colloidal stability.[16]

In both the direct and inverse methods, various parameters were studied to evaluate their effects on particle size and dispersity. For the direct method, injection rate (50, 200, and 400 μL min^{-1}), solvent to non-solvent ratio, substitution of DMSO with DMF (the solvent for PSI), as well as ethanol content of the medium did not show any significant change in the particle size and stability. Substitution of water with absolute ethanol as the medium is of great interest as such anhydrous media may provide suitable conditions for the encapsulation of water soluble or hydrolytically unstable species/agents.[17] Such a substitution, though ineffective in the direct method, significantly increased the size and narrowed the stability range in the inverse method. Stability in the inverse method was achieved only up to a concentration of 0.625 wt% when the medium was absolute ethanol (Table S2, ESI†). The large size and low colloidal stability could be attributed to low dielectric constant (*i.e.*, polarity) of the medium, lowering hydration efficiency of the ionic species which are responsible for stability.[17–20] Such a low stability was also confirmed when the ethanol content of the medium was varied at constant PSI concentration of 1.25 wt% (Table S3, ESI†). It should be added that the incorporation of polyvinyl alcohol, Tween80, Tween20, and sodium dodecyl sulfate as colloidal stabilizers (2.5 wt% with respect to polymer content) in both methods was ineffective in tuning the size, stability and shape.

Dissolution of PSI NPs and its derivatives

To assess the PSI-to-PASP conversion, dissolution of the PSI NPs was evaluated at different pH values as a function of time at 37 °C by *in situ* UV-vis spectrophotometry in terms of OD (*i.e.*, absorbance or turbidity) (Fig. 3A). PSI is insoluble in water and the nanoparticles are of a size that significantly scatters visible light, whereas PASP is a water-soluble polymer and thus its solution is transparent. Therefore, complete hydrolysis can be interpreted as being at an OD value of zero which is equal to that of water or a solution of PASP. As seen in Fig. 3A, the PSI NPs are stable under acidic conditions (pH 4.8), and the OD remains nearly constant over time. However, the OD decreases in PBS with a pH of 7.4 and gradually reaches to zero after around 16 h, suggesting complete disintegration and

dissolution of the particles. In other words, hydrophobic PSI is hydrolyzed to water-soluble PASP slowly under physiological conditions (pH = 7.4, T = 37 °C). A higher rate of dissolution was observed when the pH was increased to 8, resulting in the complete dissolution after only 6 h. Obviously, higher temperatures could further accelerate the hydrolysis. Considering relatively low colloidal stability under acidic condition (zeta potential of −15 mV at pH 3) and given the tendency of NPs to hydrolysis under neutral conditions (*i.e.*, pH 7.4), pH 5 to 6 as well as low temperatures (above zero) is recommended for the long-term storage of the PSI NPs. It should be noted that the prepared NPs were highly unstable after one cycle of freezing-thawing.

Prolonging the dissolution is of utmost importance in intravenous administration so that NPs have sufficient time for circulation and targeting before they disintegrate. Exploring various strategies (Fig. S4, ESI†), it was found that modification of PSI with EDA (2.5 mol%) as a cross-linker for PSI, or modification with OA (30 mol%) can delay the initiation of dissolution by nearly 4 and 12 h, respectively (Fig. 3B). The overall dissolution was also significantly prolonged in the case of OA modification to around 36 h. The delayed dissolution can be attributed to the incomplete network formation by EDA in the former, and the increased hydrophobicity as well as lower water diffusion in the latter. While the OD value plateaus at around 36 h for PSI-OA30, it does not reach zero, even at longer times and a slight turbidity was observed which could be due to self-association of OA units. The dissolution kinetics can also be evaluated by the first derivative of OD *vs.* times as presented in Fig. 3C. The changes in particles in terms of colloidal stability and dissolution at different pH ranges are schematically depicted in Fig. 3D.

To confirm the changes in chemical structure of the polymer, and to follow the hydrolysis reaction, the NPs were incubated under physiological conditions (PBS pH = 7.4, T = 37 °C) and at different time points, a sample was taken from the solution,

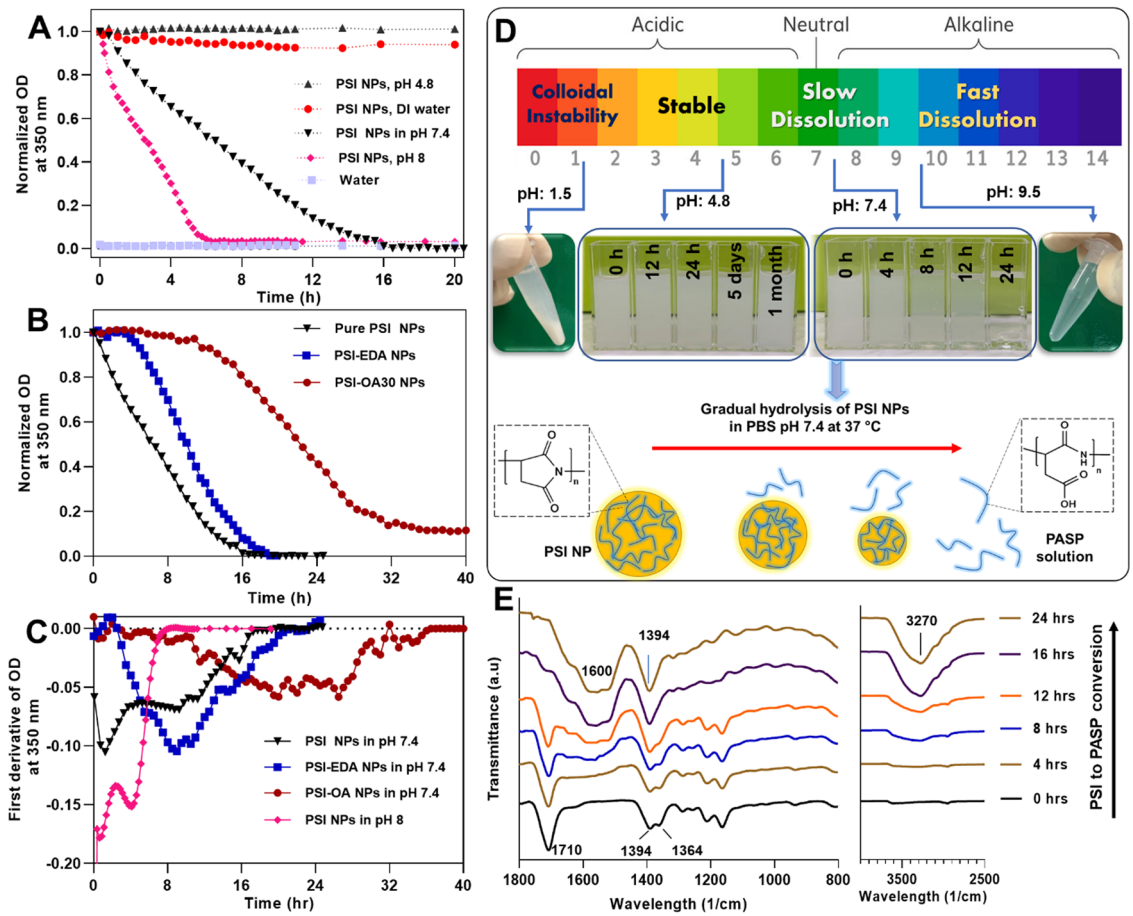

Fig. 3 Dissolution of PSI-based NPs. (A) Normalized OD (at 350 nm) of PSI NPs at 37 °C as a function of time at different pH values. (B) Normalized OD of PSI NPs, PSI-OA NPs, and PSI-EDA NPs in PBS pH 7.4 at 37 °C. Delayed dissolution of PSI-based NPs is achieved by either EDA cross-linking or PSI modification with 30 mol% of OA. PSI-OA30 NPs were prepared by pre-modification of PSI with 30 mol% of OA. PSI-EDA NPs were prepared by cross-linking of PSI with 2.5 mol% of EDA. The initiation of dissolution for PSI-OA30, and PSI-EDA2.5 is delayed by around 12, and 4 h, respectively. (C) First derivative of OD *vs.* time representing the dissolution kinetic, where PSI NPs at pH 8 showed the fastest dissolution rate (*i.e.*, the lowest value). (D) Schematic representation of PSI NPs dissolution and hydrolysis to PASP under physiological condition. (E) FTIR spectra of PSI NPs incubated under physiological condition (pH = 7.4, T = 37 °C) at different stages shows change of chemical structure from PSI to PASP; left panel is wavelength ranging from 800 to 1800 cm^{-1} while the right panel is from 2500 to 4000 cm^{-1}.

dried and analyzed by FTIR (Fig. 3E). A broad peak centered at 3270 cm^{-1}, which is attributed to the NH of the amide in PASP. In addition, a broad peak at 1600 cm^{-1} related to the amide vibrations of PASP appeared. In contrast, the peaks at around 1715 and 1790 cm^{-1} attributed to the cyclic imide carbonyls (*i.e.*, C═O) of PSI completely disappeared after hydrolysis.[6] These spectra clearly suggest the PSI-to-PASP conversion over the course of incubation.

Biocompatibility and hemocompatibility of PSI NPs

The hemolytic potential of the PSI NPs was evaluated at different concentrations after 4 h of incubation to assess their hemocompatibility for intravenous administration. Triton X-100 was used as a positive control. As a strong emulsifier, Triton X-100 lyses the red blood cell membrane (by dissolution of membrane lipid) and leads to rapid and complete hemolysis. The hemolysis percentage even at high concentrations of PSI NPs (1000 μg mL^{-1}) is less than 1%, confirming their hemocompatibility (Fig. 4A). Bender *et al.*[21] observed slight hemolysis of chitosan-coated polycaprolactone NPs, which was attributed to positive charges and residual polysorbate 80 employed in the preparation process. Basically, negatively charged NPs are repelled by the negatively charged cell membrane, preventing disruption in the cell membrane.[22] The high hemocompatibility of the PSI NPs could be due to their anionic charge as well as the absence of any stabilizer during preparation, which ensures purity of the NPs.

The PSI NPs were also found to be highly compatible with different cell lines including MOVAS, an SVEC, and macrophages J774 up to high concentration of 1000 μg mL^{-1} (Fig. 4B). Live/dead cells assay showed almost no cell death (red color in fluorescence images) upon treatment with the NPs (Fig. 4C, and Fig. S5 with larger magnification). *In vitro* and *in vivo* biocompatibility of PASP-based materials have been attributed to their protein-like structure in the backbone as an acidic polypeptide.[3,23,24] PASP was found to have very low toxicity to 3T3 fibroblasts and PC-3 cells (prostate cancer cell) with IC_{50} > 3 mg mL^{-1}.[23] PASP-based hydrogels have also been employed efficiently as scaffolds for cultivation of osteoblasts (MG-63), further verifying PASP biocompatibility.[24] Of note is that the evaluation of biocompatibility of PSI by itself is almost impossible due to its inevitable and unstoppable dissolution to PASP under cell culture conditions (pH 7.2-7.4, T = 37 °C), and therefore, one could interpret these results as biocompatibility of PASP rather than PSI NPs. However, an obvious conclusion is that the dissolution process doesn't adversely affected the cell viability or hemocompatibility.

PSI NPs as potential carriers for oral delivery of therapeutic agents to colon

Due to its inherent dissolution profile demonstrated above, PSI-based NPs can be regarded as a promising candidate for oral delivery, and a potential alternative for Eudragit which is

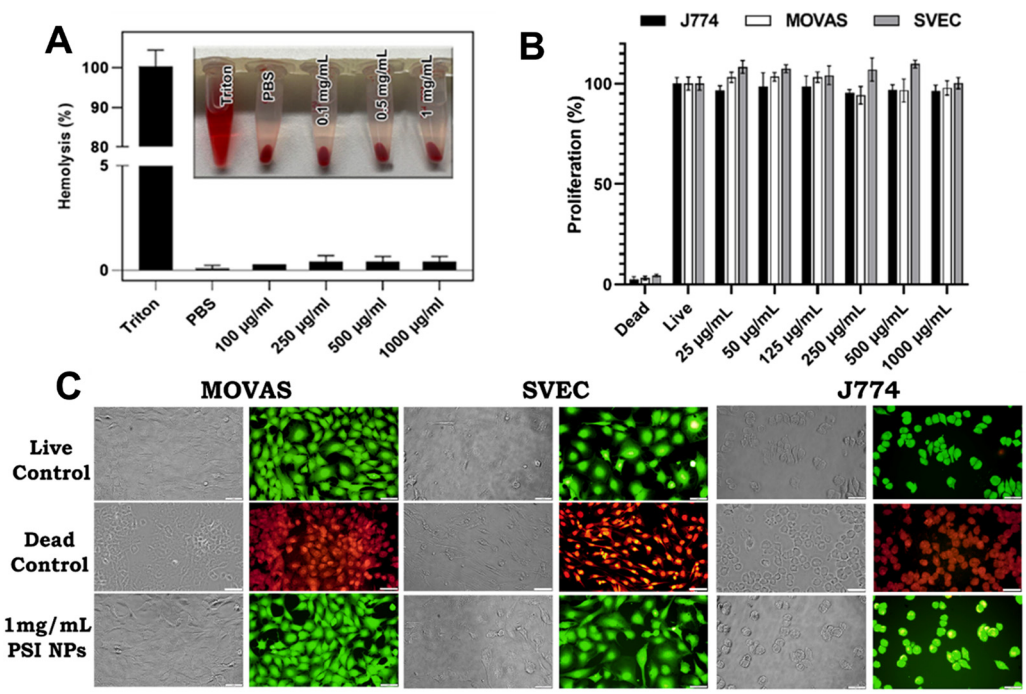

Fig. 4 Biocompatibility study of PSI NPs. (a) Hemocompatibility of the PSI NPs at different concentrations. The inset shows the photographs of the centrifuged blood after incubation with the NPs. An average of 3 replicates are presented. There is no statistically significant change based on two-way ANOVA, by comparing PBS with 1000 μg mL^{-1} treatment groups (b) Viability of MOVAS, SVEC, and macrophage (J 774) cells upon treatment with PSI NPs at different concentrations ranging from 25 to 1000 μg mL^{-1}. An average of 6 replicates are presented, where no statistically significant change was detected comparing live control and 1000 g mL^{-1} treatment group. (c) Optical microscopic images (brightfield and fluorescence, respectively on the left and right) of the cells treated with growth medium (live control), 30% of methanol (dead control), and 1 mg mL^{-1} of the NPs. The scale bars in all images are 100 μm.

a non-degradable acrylic-based polymer currently used for oral administration drug delivery.[25–27] Owing to the stability at acidic pH conditions, PSI NPs can remain stable in the stomach, protecting the payload and susceptible/degradable bioactive agents. However, after passing the stomach, as the pH increases, the particles slowly dissolve and release the payload (conjugated and un-conjugated) in the small intestine and colon. In the following experiment, Cy5 (a fluorophore) as a model molecule was chemically attached to the backbone of PSI chains, followed by NP formation. The prepared NPs were incubated at different pH conditions at 37 °C. As seen, Cy5 was gradually released over 20 h at pH 7.4, while at acidic pH, no release occurred (Fig. 5). The release profile of Cy5-PASP is in a good agreement with the dissolution profile of the PSI NPs shown in Fig. 3. Such behavior could be highly useful in treating colon-related diseases such as colon cancer. It should be added that the transit time as well as the pH reported in the literature are highly variable, as they strongly depend on the bowel evacuation conditions.[28] Despite the variations, such release behavior could still be highly useful in treating colon-related diseases such as colon cancer. Future studies could focus on simple physical loading of different therapeutic agents without chemical grafting. Precipitation methods could potentially lead to a low encapsulation efficiency and thus emulsion-based techniques should be adopted, which will be discussed in our future studies.

Sustained iron chelation of PSI NPs prevents Fenton reaction

Strong iron chelation of PASP has already been demonstrated and reviewed by us.[2] The chelation process typically occurs quickly. Fast chelation could be detrimental because the administration of the chelating agent could suddenly reduce the concentration of free essential ions in circulation. PSI NPs slowly release PASP under the physiological condition, so they could be beneficial for sustained chelation. To evaluate this behavior, iron chelation of PSI NPs was evaluated at different incubation times. The NPs were incubated at pH 7.4 at 37 °C for

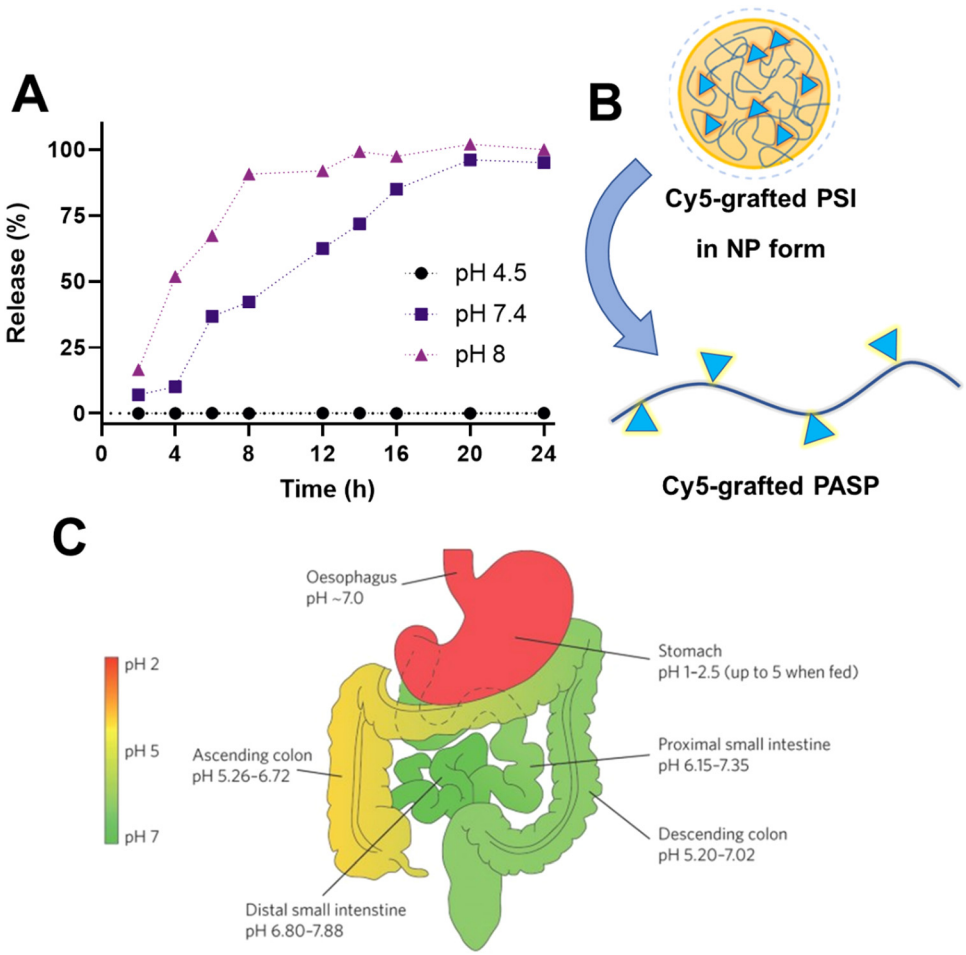

Fig. 5 Nanoparticles of drug-conjugated PSI as a potential system for delivery/release of susceptible agent to large and small intestine. (A) Release of Cy5-conjugated PSI NPs at different pH conditions at 37 °C. Cy5 was chemically attached on PSI polymer backbone followed by nano-precipitation method to prepare the NPs. The NPs were stable at pH 4.5, maintaining Cy5 in its structure, while by increasing pH, Cy5-modified PASP was released from the NPs. (B) Schematic representation of release process, where NPs of Cy-5-conjugated PSI are hydrolyzed to water soluble Cy5-PASP. (C) Schematic representation of human gastrointestinal tract and pH values at different parts. Figure adapted with permission from ref. 28. The transit times for the oesophagus is 10–14 seconds. For the small intestine, it is approx. 3–5 h, whereas for the colon, it is highly variable, based on bowel condition.

different time intervals followed by the addition of iron, H_2O_2 and ABTS. As seen in Fig. 6, the absorbance at 414 nm reduced over time. It should be noted that PSI itself has no activity in lowering the oxidation of ABTS as the absorbance at 414 with and without PSI NPs were almost identical. The lower absorbance value at longer PSI incubation reflected the fact that PASP was released from the NPs, chelated iron and thus stopped ABTS oxidation. After incubation of PSI NPs for 24 h (equivalent to complete hydrolysis of the particles, and conversion to PASP), complete inhibition of the oxidation reaction was observed and thus no color was generated by the addition of H_2O_2 and ABTS. Such sustained iron chelation by PSI NPs could be beneficial for lowering reactive oxygen species (ROS) and reducing iron toxicity. Hydroxyl radicals are known as the strongest ROS that can damage cell and DNA through oxidation.[29] The hydroxyl radicals are generated by the Fenton reaction which is catalyzed by iron ions (eqn (1) and (2)). As such, PASP could suppress the Fenton reaction by iron chelation (eqn (3) and (4)). The data from this experiment further confirm the sustained release of PASP from PSI NPs.

$$Fe^{2+} + H_2O_2 \rightarrow Fe^{3+} + {}^{\bullet}OH + OH^{-} \quad (1)$$

$$Fe^{3+} + H_2O_2 \rightarrow Fe^{2+} + {}^{\bullet}OOH + H^{+} \quad (2)$$

$$Fe^{2+} + PASP + H_2O_2 \rightarrow [Fe^{2+}\_PASP] + H_2O_2 \quad (3)$$

$$Fe^{3+} + PASP + H_2O_2 \rightarrow [Fe^{3+}\_PASP] + H_2O_2 \quad (4)$$

$$ABTS + {}^{\bullet}OH \rightarrow ABTS^{\bullet+} \quad \text{blue color/absorbance 414 nm} \quad (5)$$

Prevention of calcification of vascular smooth muscle cells by PSI NPs

PASP has a high affinity toward different metal ions such as calcium and iron whose high concentrations are correlated to soft-tissue calcification and cancer, respectively.[30,31] Vascular calcification is the main cause of death in patients with chronic kidney diseases and its etiology is correlated to high serum levels of calcium phosphate because of kidney dysfunction. VSMCs are the main mediator for vascular calcification because they trans-differentiate into osteogenic cells under pathological conditions, facilitating calcium deposition.[32–34] A variety of studies have shown that the chelation ability of PASP results in the prevention of calcium precipitation and deposition.[2] Considering these results, we expect that because PASP is spontaneously synthesized by the gradual hydrolysis of PSI NPs, calcification of VSMCs would be prevented. Therefore, herein the effect of PSI NPs on *in vitro* calcification of MOVAS (a type of VSMCs isolated from mouse aorta) is evaluated.

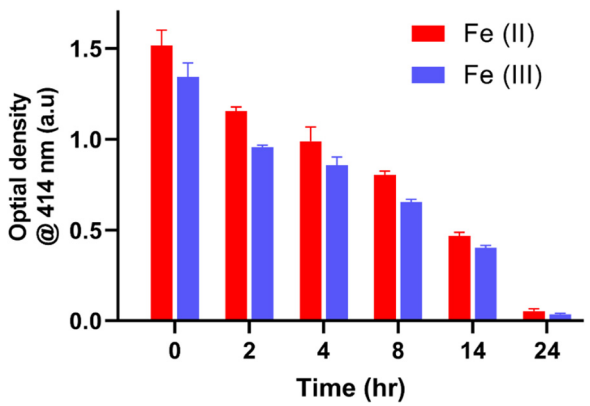

Fig. 6 Sustained iron chelation of PSI NPs. OD at 414 nm for the PSI NPs samples taken after different incubation time. The higher the OD corresponds to higher level of ABTS oxidation. Pure PSI NPs has no activity in lowering the oxidation of ABTS. However, incubation of the NPs under physiological condition generates PASP, a strong iron chelator, thereby reducing ABTS oxidation through blocking the Fenton reaction.

Incubation of MOVAS for 12 days (4 × 3 days) in calcification media (DMEM supplemented with 10 mM βGP and 1 mM $CaCl_2$, 50 μg mL^{-1} L-ascorbic acid) led to extensive mineralization. Such a culture condition was found to increase the level of calcium deposition by around 8 times (Fig. 7A). This is attributed to the trans-differentiation of MOVAS to osteogenic cells, thereby upregulating bone gene markers such as ALP (Fig. 7B).[32,33] ALP is a well-known enzyme that catalyzes the hydrolysis of pyrophosphates to inorganic phosphate. While the former is regarded as a potent inhibitor, the latter serves as an inducer for calcium deposition.

As seen in Fig. 7B, the ALP activity in the cells treated with calcification inducers was significantly higher than that in the control group. The presence of PSI NPs, though ineffective in reducing the ALP level, inhibited calcification particularly at concentrations ≥ 50 μg mL^{-1}. The calcium deposition, however, was not significantly affected at low concentrations (10 μg mL^{-1}, Fig. 7A). However, as low as 50 μg mL^{-1} reduced calcification by more than 4 times compared to the βGP control. Increasing the PSI NPs concentration to 100 μg mL^{-1} further attenuated the calcium level almost to that of the negative control (*i.e.*, normal culture without βGP). Staining of the cells with Alizarin red which stained calcium deposits red, verified the quantitative measurement (Fig. 7C). The viability of MOVAS after 12 days of incubation was assessed quantitatively by PrestoBlue (Fig. S6A, ESI†) and qualitatively by live/dead cell staining assays (Fig. S6B, ESI†), suggesting that PSI NPs do not affect the cell viability significantly which further confirms the biocompatibility results shown in Fig. 4.

Conclusion

In summary, well-defined PSI NPs with tunable sizes were prepared without the use of a stabilizer. The PSI NPs were non-toxic to cells and exhibited excellent hemocompatibility at concentrations up to 1 mg mL^{-1}. It was demonstrated that the NPs remain stable under acidic conditions, while converting to PASP slowly under physiological conditions (37 °C, pH 7.4). Dissolution of the NPs under neutral conditions and their stability under acidic environments is a highly desirable feature for oral delivery systems. The dissolution rate could be tuned through chemical modification of PSI. The delayed dissolution is expected to benefit a wide range of drug delivery applications.

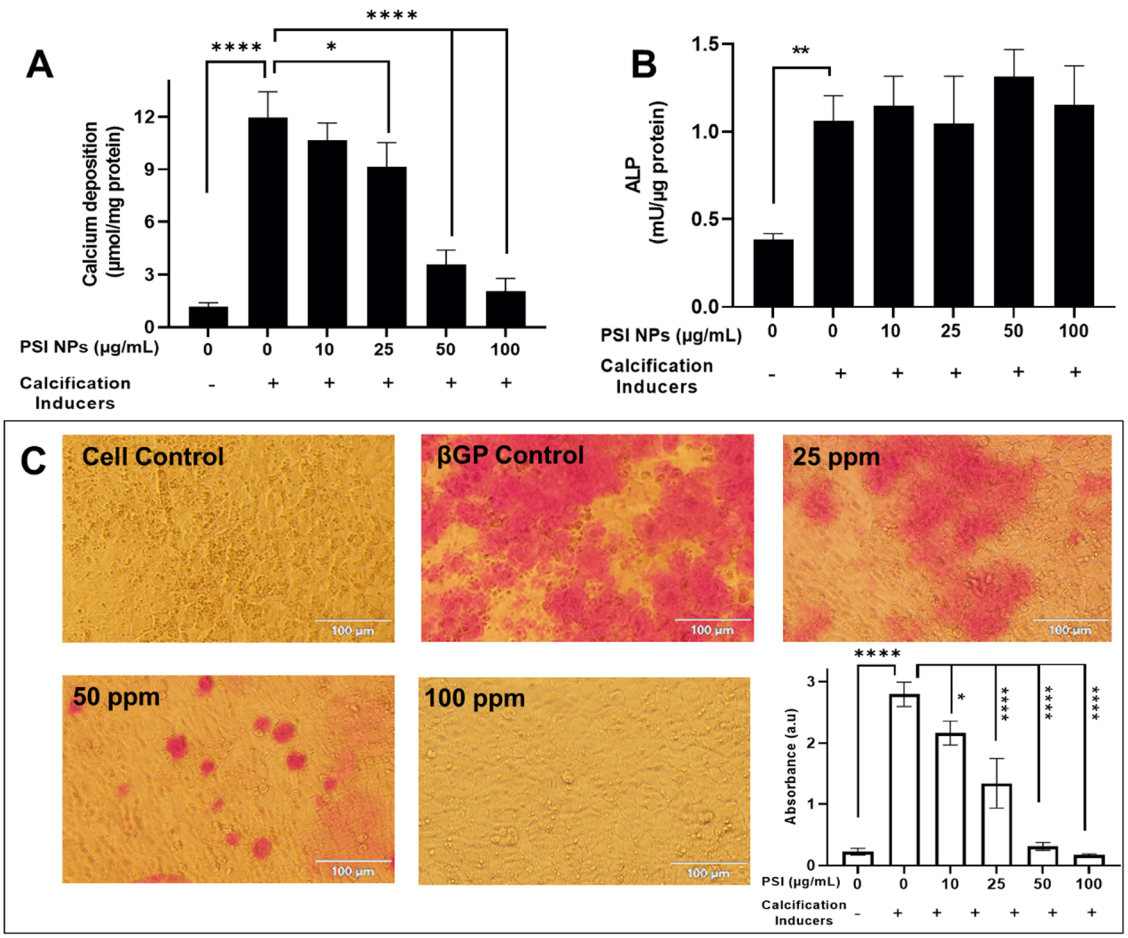

Fig. 7 *In vitro* calcification of MOVAS. (A) The amount of deposited calcium normalized to protein content after 12 days of incubation with calcification inducers shows that PSI NPs effectively inhibited calcium deposition. (B) ALP activity of MOVAS after 12 days of incubation with calcification inducers indicates that ALP was upregulated, and that PSI NPs did not affect ALP activity. The statistical analysis comparison was carried out with respect to cells treated with calcification inducers without PSI NPs (C) Calcium deposition under different concentrations of PSI NPs. Alizarin red staining of the cells shows large calcium deposits in red color. "Cell control" is cells without any treatment, whereas "βGP control" is cells treated with calcification inducers in the absence of the NPs. The graph shows the extent of calcium measured (absorbance at 414 nm) through dissolution of calcium-alizarin red by acetic acid solution. Scale bar in the images is 100 μm. Data are presented as mean ± SD of at least 3 replicates. n.s. (not significant) $P > 0.05$. *$P < 0.05$, **$P < 0.01$, ***$P < 0.001$, ****$P < 0.0001$.

As a model molecule, Cy5, as a fluorophore, was grafted onto PSI chain, and the corresponding particles were formed. The release of Cy5-grafted PASP was demonstrated under neutral and slightly alkaline conditions, suggesting their potential for developing nanoparticle drugs for the treatment of colon-related diseases. Furthermore, PSI NPs may reasonably be viewed as being reservoirs for spontaneous and sustained release of PASP under physiological conditions. This offers various unexplored applications in several biomedical areas because the ASP moiety in different proteins (*e.g.*, osteopontin, and transferrin) can carry out key functions in regulation of metal ions. With that in mind and considering the biocompatibility and biodegradability of PASP as a bioactive polypeptide, we showed that PSI NPs prevent *in vitro* calcification of smooth muscle cells. Sustained iron chelation of PSI NPs over 20 h was also demonstrated, which could find potential in the prevention ROS generation through blocking the Fenton reaction. Moving ahead, there will certainly be more potentials to be exploited and more challenges to be solved.

Conflicts of interest

There are no conflicts to declare.

Acknowledgements

This work is funded by National Health and Medical Research Council (HTT: APP1037310, APP1182347, APP2002827) and Heart Foundation (HTT: 102761). The authors would like to acknowledge the Australian National Fabrication Facility (Queensland Node) for access to key items of equipment.

References

1 P. S. Yavvari, A. K. Awasthi, A. Sharma, A. Bajaj and A. Srivastava, Emerging biomedical applications of poly-aspartic acid-derived biodegradable polyelectrolytes and polyelectrolyte complexes, *J. Mater. Chem. B*, 2019, **7**(13), 2102–2122.

2 H. Adelnia, F. Sirous, I. Blakey and H. T. Ta, Metal ion chelation of poly(aspartic acid): From scale inhibition to therapeutic potentials, *Int. J. Biol. Macromol.*, 2022, **229**, 974–993.

3 H. Adelnia, I. Blakey, P. J. Little and H. T. Ta, Hydrogels based on poly(aspartic acid): Synthesis and applications, *Front. Chem.*, 2019, 755.

4 G. Zhang, H. Yi and C. Bao, Stimuli-Responsive Poly(aspartamide) Derivatives and Their Applications as Drug Carriers, *Int. J. Mol. Sci.*, 2021, **22**(16), 8817.

5 E. Jalalvandi and A. Shavandi, Polysuccinimide and its derivatives: Degradable and water soluble polymers, *Eur. Polym. J.*, 2018, **109**, 43–54.

6 H. Adelnia, H. D. Tran, P. J. Little, I. Blakey and H. T. Ta, Poly(aspartic acid) in biomedical applications: From polymerization, modification, properties, degradation, and biocompatibility to applications, *ACS Biomater. Sci. Eng.*, 2021, **7**(6), 2083–2105.

7 E. Jalalvandi, L. R. Hanton and S. C. Moratti, Schiff-base based hydrogels as degradable platforms for hydrophobic drug delivery, *Eur. Polym. J.*, 2017, **90**, 13–24.

8 S. Marasini, H. Yue, A. Ghazanfari, S. L. Ho, J. A. Park and S. Kim, *et al.*, Polyaspartic Acid-Coated Paramagnetic Gadolinium Oxide Nanoparticles as a Dual-Modal T1 and T2 Magnetic Resonance Imaging Contrast Agent, *Appl. Sci.*, 2021, **11**(17), 8222.

9 Y. Chen, X. Chen, Y. Liang and Y. Gao, Synthesis of polyaspartic acid-oxidized starch copolymer and evaluation of its inhibition performance and dispersion capacity, *J. Dispersion Sci. Technol.*, 2021, **42**(13), 1926–1935.

10 S. Zakharchenko, E. Sperling and L. Ionov, Fully biodegradable self-rolled polymer tubes: a candidate for tissue engineering scaffolds, *Biomacromolecules*, 2011, **12**(6), 2211–2215.

11 C. Zhao, S. Melis, E. P. Hughes, T. Li, X. Zhang and P. D. Olmsted, *et al.*, Particle formation mechanisms in the nanoprecipitation of polystyrene, *Langmuir*, 2020, **36**(44), 13210–13217.

12 W. Huang and C. Zhang, Tuning the size of poly(lactic-*co*-glycolic acid)(PLGA) nanoparticles fabricated by nanoprecipitation, *Biotechnol. J.*, 2018, **13**(1), 1700203.

13 W. Badri, K. Miladi, Q. A. Nazari, H. Fessi and A. Elaissari, Effect of process and formulation parameters on polycaprolactone nanoparticles prepared by solvent displacement, *Colloids Surf., A*, 2017, **516**, 238–244.

14 A. Geissler, M. Biesalski, T. Heinze and K. Zhang, Formation of nanostructured cellulose stearoyl esters via nanoprecipitation, *J. Mater. Chem. A*, 2014, **2**(4), 1107–1116.

15 E. Aschenbrenner, K. Bley, K. Koynov, M. Makowski, M. Kappl and K. Landfester, *et al.*, Using the polymeric ouzo effect for the preparation of polysaccharide-based nanoparticles, *Langmuir*, 2013, **29**(28), 8845–8855.

16 I. Peinado, U. Lesmes, A. Andrés and J. D. McClements, Fabrication and morphological characterization of biopolymer particles formed by electrostatic complexation of heat treated lactoferrin and anionic polysaccharides, *Langmuir*, 2010, **26**(12), 9827–9834.

17 U. Bilati, E. Allémann and E. Doelker, Nanoprecipitation versus emulsion-based techniques for the encapsulation of proteins into biodegradable nanoparticles and process-related stability issues, *AAPS PharmSciTech*, 2005, **6**(4), E594–E604.

18 H. Adelnia, J. N. Gavgani, H. Riazi and H. C. Bidsorkhi, Transition behavior, surface characteristics and film formation of functionalized poly(methyl methacrylate-*co*-butyl acrylate) particles, *Prog. Org. Coat.*, 2014, **77**(11), 1826–1833.

19 H. Adelnia, J. N. Gavgani and M. Soheilmoghaddam, Fabrication of composite polymer particles by stabilizer-free seeded polymerization, *Colloid Polym. Sci.*, 2015, **293**(8), 2445–2450.

20 S. M. Molaei, H. Adelnia, A. M. Seif and J. Nasrollah Gavgani, Sulfonate-functionalized polyacrylonitrile-based nanoparticles; synthesis, and conversion to pH-sensitive nanogels, *Colloid Polym. Sci.*, 2019, **297**(9), 1245–1253.

21 E. A. Bender, M. D. Adorne, L. M. Colomé, D. S. Abdalla, S. S. Guterres and A. R. Pohlmann, Hemocompatibility of poly(ε-caprolactone) lipid-core nanocapsules stabilized with polysorbate 80-lecithin and uncoated or coated with chitosan, *Int. J. Pharm.*, 2012, **426**(1–2), 271–279.

22 L. Chen, J. J. Glass, R. De Rose, C. Sperling, S. J. Kent and Z. H. Houston, *et al.*, Influence of Charge on Hemocompatibility and Immunoreactivity of Polymeric Nanoparticles, *ACS Appl. Bio Mater.*, 2018, **1**(3), 756–767.

23 D. V. Salakhieva, D. Gumerova, R. Akhmadishina, M. Kamalov, I. Nizamov and C. Nemeth, *et al.*, Anti-Radical and Cytotoxic Activity of Polysuccinimide and Polyaspartic Acid of Different Molecular Weight, *Bionanoscience*, 2016, **6**(4), 348–351.

24 D. Juriga, K. Nagy, A. Jedlovszky-Hajdú, K. Perczel-Kovách, Y. M. Chen and G. Varga, *et al.*, Biodegradation and osteosarcoma cell cultivation on poly(aspartic acid) based hydrogels, *ACS Appl. Mater. Interfaces*, 2016, **8**(36), 23463–23476.

25 M. K. Anwer, R. Al-Shdefat, E. Ezzeldin, S. M. Alshahrani, A. S. Alshetaili and M. Iqbal, Preparation, evaluation and bioavailability studies of eudragit coated PLGA nanoparticles for sustained release of eluxadoline for the treatment of irritable bowel syndrome, *Front. Pharmacol.*, 2017, **8**, 844.

26 C. Y. Wong, H. Al-Salami and C. R. Dass, Microparticles, microcapsules and microspheres: a review of recent developments and prospects for oral delivery of insulin, *Int. J. Pharm.*, 2018, **537**(1–2), 223–244.

27 H. Adelnia, R. Ensandoost, S. Shebbrin Moonshi, J. N. Gavgani, E. I. Vasafi and H. T. Ta, Freeze/thawed polyvinyl alcohol hydrogels: present, past and future, *Eur. Polym. J.*, 2022, **164**, 110974.

28 V. V. Khutoryanskiy, Longer and safer gastric residence, *Nat. Mater.*, 2015, **14**(10), 963–964.

29 F. Beaufay, E. Quarles, A. Franz, O. Katamanin, W.-Y. Wholey and U. Jakob, Polyphosphate functions in vivo as an iron chelator and Fenton reaction inhibitor, *mBio*, 2020, **11**(4), e01017–e01020.

30 L. Demer Linda and Y. Tintut, Vascular Calcification, *Circulation*, 2008, **117**(22), 2938–2948.

31 S. V. Torti and F. M. Torti, Iron and cancer: more ore to be mined, *Nat. Rev. Cancer*, 2013, **13**(5), 342–355.

32 N. Skafi, D. Abdallah, C. Soulage, S. Reibel, N. Vitale and E. Hamade, *et al.*, Phospholipase D: A new mediator during high phosphate-induced vascular calcification associated with chronic kidney disease, *J. Cell. Physiol.*, 2019, **234**(4), 4825–4839.

33 N. Mackenzie, D. Zhu, L. Longley, C. Patterson, S. Kommareddy and V. MacRae, MOVAS-1 cell line: a new in vitro model of vascular calcification, *Int. J. Mol. Med.*, 2011, **27**(5), 663–668.

34 X.-Y. Li, Q.-M. Li, Q. Fang, X.-Q. Zha, L.-H. Pan and J.-P. Luo, Laminaria japonica polysaccharide inhibits vascular calcification via preventing osteoblastic differentiation of vascular smooth muscle cells, *J. Agric. Food Chem.*, 2018, **66**(8), 1821–1827.

